TECHNICAL REPORT
https://doi.org/10.1038/s41593-018-0316-9
nature neuroscience

# Differentiation and maturation of oligodendrocytes in human three-dimensional neural cultures

Rebecca M. Marton[1,2], Yuki Miura[1], Steven A. Sloan[1], Qingyun Li[3], Omer Revah[1], Rebecca J. Levy[4], John R. Huguenard[4] and Sergiu P. Pașca[1,5*]

**Investigating human oligodendrogenesis and the interaction of oligodendrocytes with neurons and astrocytes would accelerate our understanding of the mechanisms underlying white matter disorders. However, this is challenging because of the limited accessibility of functional human brain tissue. Here, we developed a new differentiation method of human induced pluripotent stem cells to generate three-dimensional brain organoids that contain oligodendrocytes as well as neurons and astrocytes, called human oligodendrocyte spheroids. We found that oligodendrocyte lineage cells derived in human oligodendrocyte spheroids transitioned through developmental stages similar to primary human oligodendrocytes and that the migration of oligodendrocyte lineage cells and their susceptibility to lysolecithin exposure could be captured by live imaging. Moreover, their morphology changed as they matured over time in vitro and started myelinating neurons. We anticipate that this method can be used to study oligodendrocyte development, myelination, and interactions with other major cell types in the CNS.**

Oligodendrocytes have key roles in brain development, including myelinating and electrically insulating neuronal axons for impulse propagation, as well as providing trophic and metabolic support for neurons[1–4]. These functions are coordinated by communication between oligodendrocytes and neighboring astrocytes and neurons[5–7], which occurs both through physical interactions and through secreted factors[5,8–11]. During neural development, oligodendrocyte lineage cells progress from mobile, bipolar oligodendrocyte progenitor cells (OPCs) to stationary, highly branched mature oligodendrocytes. The loss of oligodendrocytes or alterations in their ability to migrate, myelinate, or communicate with other cell types can lead to diseases such as multiple sclerosis and vanishing white matter disease[12,13].

Although methods have been developed to generate oligodendrocytes from human pluripotent stem cells[14–18], these models cannot be maintained long term in vitro and lack the diversity of mature cell types and the cytoarchitecture that oligodendrocytes encounter in vivo. These features of two-dimensional culture make the study of cellular interactions difficult as they occur in a three-dimensional (3D) environment in vivo. The advent of organoid methodologies has allowed the generation of self-organized cellular models with complex cytoarchitecture in vitro, and these cultures can be maintained over extended periods of time[19]. Here, we developed an approach to differentiate human induced pluripotent stem (hiPS) cells into 3D neural spheroids to model the development of human oligodendrocyte lineage cells alongside neurons and astrocytes. Our method produced human neurons, astrocytes, and oligodendrocytes that co-developed both spatially and temporally. The oligodendrocytes transitioned through developmental stages and were transcriptionally similar to primary oligodendrocytes. Oligodendrocyte lineage cells matured morphologically and electrophysiologically over time and ultimately myelinated nearby axons.

## Results

**Generation and characterization of human oligodendrocyte spheroids (hOLS).** To generate hOLS that contain oligodendrocytes, astrocytes, and neurons, we leveraged approaches to derive region-specific 3D cultures that we previously developed[20,21]. We enzymatically dissociated hiPS cells into a single cell suspension ($n=7$ hiPS cell lines derived from 7 control subjects; see Supplementary Table 1) and aggregated them into spheroids using microwells (Fig. 1a). After dislodging the spheroids from the microwells 18–24 h later, we exposed them to dual SMAD inhibitors dorsomorphin and SB-431542 followed by epidermal growth factor (EGF) and fibroblast growth factor 2. Smoothened agonist and IWP-2 were added to activate the SHH pathway (days 12–24) and inhibit the WNT pathway (days 4–24), respectively. From day 25 to day 36, we added platelet-derived growth factor (PDGF), hepatocyte growth factor, insulin-like growth factor 1, neurotrophin 3 (NT-3), brain-derived neurotrophic factor (BDNF), insulin, triiodo-L-thyronine (T3), biotin, and a cyclic AMP analog (cAMP) to promote OPC survival and proliferation[14]. At day 37, insulin, biotin, T3, cAMP, and L-ascorbic acid were added to the media for the duration of culture to promote oligodendrocyte maturation. At day 25 of in vitro culture, hOLS showed high expression of the ectoderm marker *SOX2*, but not the mesoderm or endoderm markers *BRACH* and *SOX17* (Supplementary Fig. 1a; $n=4$ samples from hOLS derived from 4 hiPS cell lines). At day 37, hOLS expressed the forebrain markers *FOXG1*, *SIX3*, *NKX2-1*, *OTX2*, *PAX6*, and *LHX2* at levels comparable to or higher than our previously described method to generate human cortical spheroids (hCS)[20,22], but not midbrain- (*LMX1B*), hypothalamus- (*RAX*), or spinal cord- (*HOXB4*) related genes (Supplementary Fig. 1b; $n=5$ samples from hOLS derived from 5 hiPS cell lines).

At day 100 of in vitro differentiation, we found a significant increase in gene expression of *OLIG2*, *NKX2-2*, and *MBP* in hOLS as

[1]Department of Psychiatry and Behavioral Sciences, Stanford University School of Medicine, Stanford, CA, USA. [2]Program in Stem Cell Biology and Regenerative Medicine, Stanford University School of Medicine, Stanford, CA, USA. [3]Department of Neurobiology, Stanford University School of Medicine, Stanford, CA, USA. [4]Department of Neurology and Neurological Sciences, Stanford University School of Medicine, Stanford, CA, USA. [5]Human Brain Organogenesis Program, Stanford University, Stanford, CA, USA. *e-mail: spasca@stanford.edu

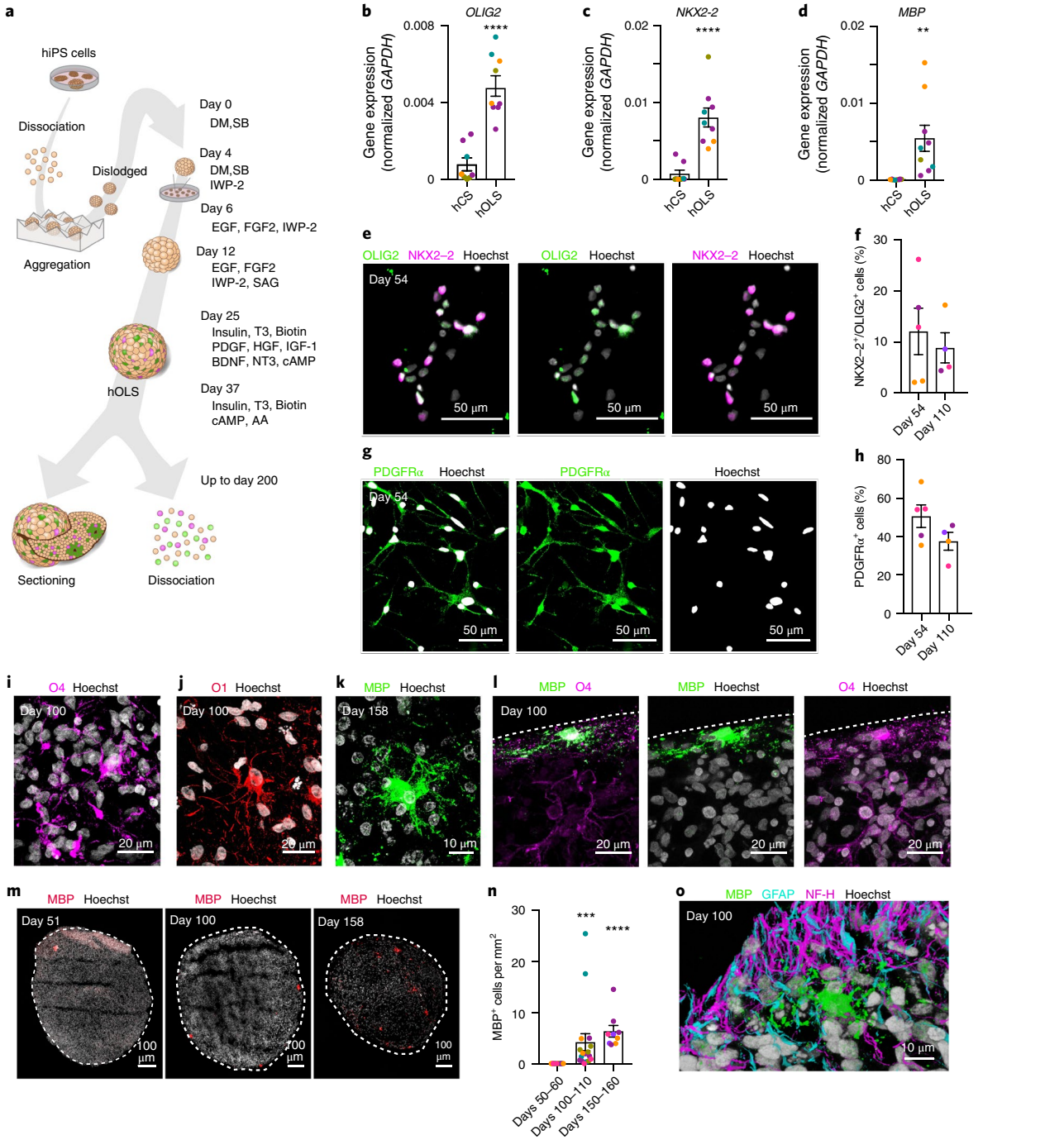


**Fig. 1 | Characterization of hOLS derived from hiPS cell lines. a**, Schematic for generating hOLS. hiPS cells are enzymatically dissociated and aggregated in microwells to form spheroids. DM, dorsomorphin; SB, SB-431542; SAG, smoothened agonist; HGF, hepatocyte growth factor; AA, ascorbic acid. **b**–**d**, Relative gene expression (normalized to *GAPDH*) as determined by qPCR at day 100 of in vitro culture in hCS and hOLS of *OLIG2* (**b**) (two-tailed Mann–Whitney test, $^{****}P < 0.0001$), *NKX2-2* (**c**) (two-tailed Mann–Whitney test, $^{****}P < 0.0001$), and *MBP* (**d**) (two-tailed *t* test, $t = 2.97$, d.f. = 15, $^{***}P = 0.009$). In **b**–**d**, for hCS $n = 8$ and for hOLS $n = 9$ RNA samples from spheroids derived from 4 hiPS cell lines in 1–4 differentiation experiments; see Supplementary Table 1. Lines are shown in different colors; each point represents 2–4 hOLS pooled from 1 differentiation experiment. **e**–**h**, Day 54 immunostaining and quantification of OLIG2 and NKX2-2 double-positive cells (**e**,**f**) (two-tailed *t* test, $t = 0.55$, d.f. = 7, $P = 0.59$) and of PDGFRα (**g**,**h**) (two-tailed *t* test, $t = 1.68$, d.f. = 7, $P = 0.13$) out of Hoechst in dissociated hOLS at day 54 and day 110 ($n = 5$ samples each consisting of 4–6 hOLS derived from 3 hiPS cell lines; hiPS cell lines shown in different colors; see Supplementary Table 1). **i**–**l**, Immunostaining of O4 (**i**), O1 (**j**), MBP (**k**), and MBP and O4 (**l**) in cryosections. Immunostainings were repeated on hOLS from six independent inductions for O4, three independent inductions for O1, five independent inductions for MBP, and three independent inductions for MBP and O4 together with similar results. **m**,**n**, Immunostaining (**m**) and quantification (**n**) of $MBP^+$ cells over time in whole hOLS cryosections (days 50–60: $n = 12$ hOLS from 5 hiPS cell lines; days 100–110: $n = 17$ hOLS from 5 hiPS cell lines; days 150–160: $n = 9$ hOLS from 4 hiPS cell lines; each point represents one hOLS; see Supplementary Table 1; Kruskal–Wallis test, $P < 0.0001$ with Dunn's multiple comparison test days 50–60 versus days 100–110, $^{***}P = 0.0005$, and days 50–60 versus days 100–110, $^{****}P < 0.0001$). **o**, Immunostaining of MBP, GFAP, and NF-H in hOLS cryosections. Immunostainings were repeated on hOLS from three independent inductions with similar results. Data are mean ± s.e.m. Scale bars, 10 µm (**k**,**o**), 20 µm (**i**,**j**,**l**), 50 µm (**e**,**g**), and 100 µm (**m**).

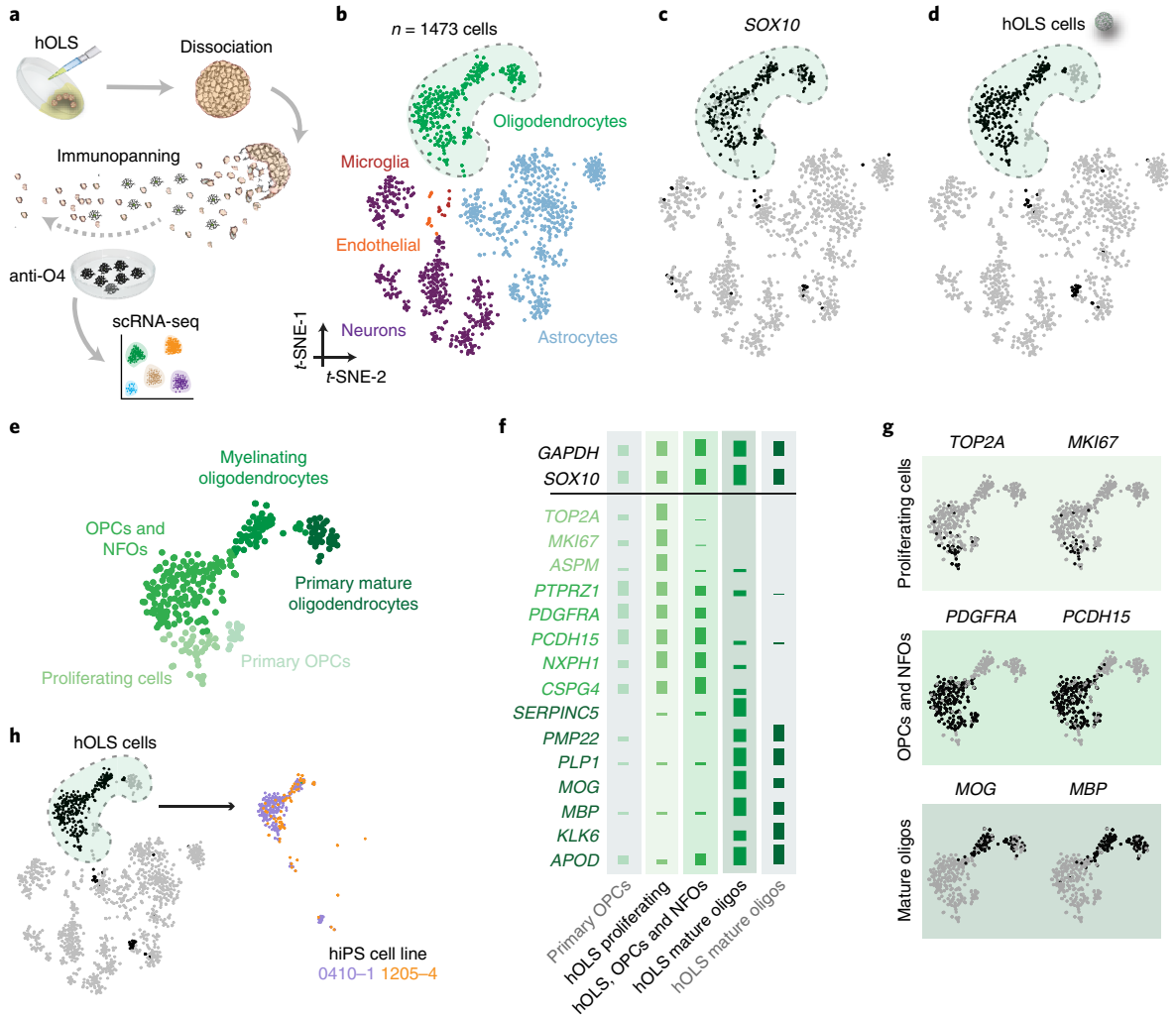


**Fig. 2 | Transcriptional comparison of hOLS oligodendrocyte lineage cells to primary tissue cells. a**, Schematic showing the isolation of O4$^+$ cells from hOLS. scRNA-seq, single-cell RNA-sequencing. **b**, *t*-SNE clustering data from hOLS ($n=295$ cells), primary human brain tissue, and hCS ($n=1,473$ cells total; colored by cell type). **c**, Gene expression of oligodendrocyte lineage-related *SOX10* in single cells. **d**, O4$^+$ hOLS-derived single cells. **e**, Oligodendrocyte cluster from *t*-SNE map in **b** with three distinct *k*-means subclusters of hOLS. **f**, Mean expression of oligodendrocyte-lineage-specific genes in hOLS as well as primary OPCs and mature oligodendrocytes isolated from adult human brain tissue ($\log_2$ data normalized across rows). **g**, Single-cell gene expression of subcluster-specific markers in the oligodendrocyte lineage cluster. **h**, O4$^+$ single cells derived from hOLS indicated by hiPS cell line.

determined by quantitative PCR (qPCR) compared with hCS[20], suggesting an enrichment of oligodendrocyte lineage cells ($n=9$ samples from hOLS and $n=8$ samples from hCS derived from 4 hiPS cell lines; $P<0.001$; Fig. 1b–d). We next performed immunofluorescent labeling on cryosections (Supplementary Fig. 1c) obtained at day 51 and dissociated cultures obtained from day 54 and day 110 hOLS to test for the presence of NKX2-2$^+$/OLIG2$^+$ double-positive OPCs and PDGFRα$^+$ OPCs (Fig. 1e–h). Approximately 12% of cells at day 54 and 9% of cells at day 110 were NKX2-2$^+$/OLIG2$^+$ double-positive (Fig. 1f; $n=4–5$ samples from hOLS derived from 3 hiPS cell lines) and approximately 51% of cells at day 54 and 35% of cells at day 110 were PDGFRα$^+$ (Fig. 1h; $n=4–5$ samples from hOLS derived from 3 hiPS cell lines). To determine whether OPCs were maturing into oligodendrocytes over time, we immunostained cryosections obtained from hOLS at days 100–160 of in vitro differentiation. We observed O4$^+$, O1$^+$, and MBP$^+$ cells, indicating a range of oligodendrocyte stages from pre-oligodendrocytes to mature, late-stage oligodendrocytes (Fig. 1i–k). Notably, we found both O4$^+$ cells that were bipolar and did not express MBP, as well as O4$^+$ cells that were highly branched and overlapped with MBP (Fig. 1l). To determine whether the abundance of mature oligodendrocytes increased in hOLS over time, we quantified the density of MBP$^+$ cells in whole cryosections between days 50 and 160 of differentiation. We observed an increase in the density of MBP$^+$ cells and that most MBP$^+$ cells were located in the outer third of each section (Fig. 1m,n and Supplementary Fig. 1d; $n=9–17$ hOLS from 6 hiPS cell lines; $P<0.0001$).

A goal of this method was to produce oligodendrocytes in close proximity to neurons and astrocytes, so we performed immunostainings in day 100 hOLS cryosections for MBP, GFAP, and Neurofilament-H (200 kD) (NF-H). We observed both neurons and glial lineage cells in close proximity to each other (Fig. 1o). Moreover, the relative gene expression of the neural marker *RBFOX3* as determined by qPCR at day 100 was comparable between hCS and hOLS (Supplementary Fig. 1e; $P>0.05$), whereas the glial marker *GFAP* was expressed at a higher level in hOLS (Supplementary Fig. 1e; $P<0.01$). Quantifications in dissociated cultures revealed that approximately 45% of cells at day 54 and 20% of cells at day 110 were MAP2$^+$, and 8% of cells at day 54 and 21% of cells at day 110 were GFAP$^+$ (Supplementary Fig. 1f–i; $n=4–5$ samples from hOLS from 3 hiPS cell lines). To verify neurotransmitter identity in these cultures, we next used qPCR and found that hOLS expressed

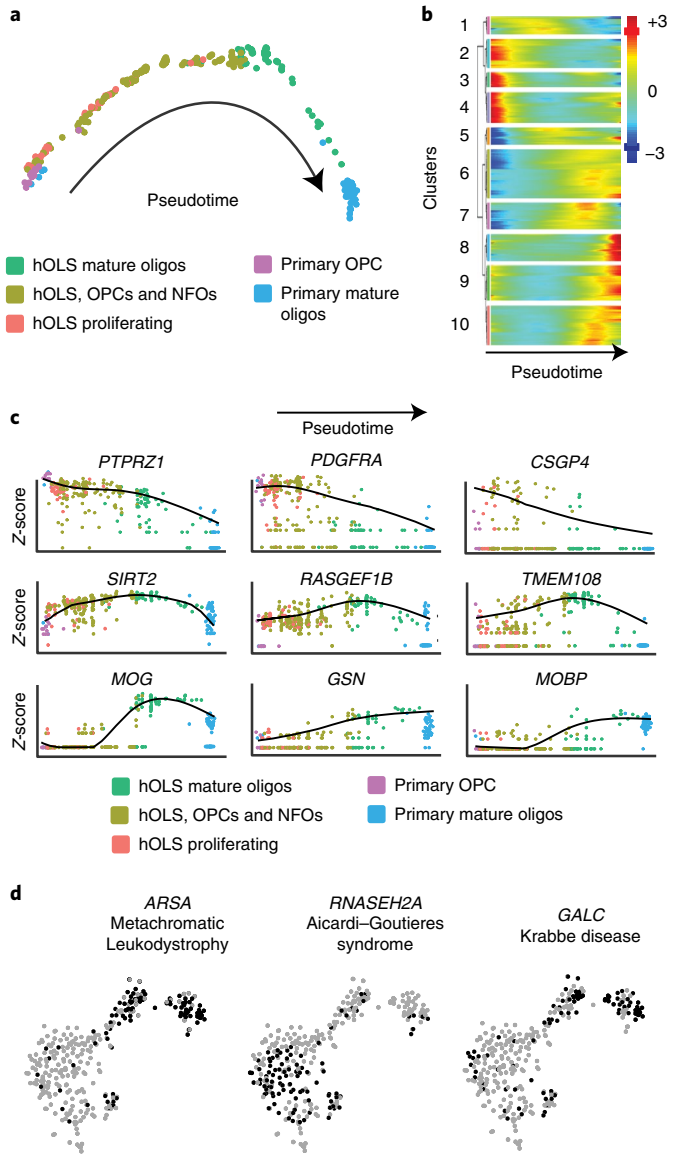


**Fig. 3 | Developmental trajectory and expression of disease-related genes in hOLS. a**, Monocle pseudotime analysis of all oligodendrocyte lineage cells colored by tissue of origin. Most mature time points are shown on right. **b**, Hierarchical clustered heat map depicting gene modules whose expression patterns co-vary across pseudotime (*z*-scores normalized by row). **c**, Expression of oligodendrocyte lineage markers across pseudotime (colored by tissue of origin; $\log_2$ data normalized by gene). **d**, Singe-cell gene expression pattern of disease-implicated genes in the oligodendrocyte lineage cluster from (Fig. 2b).

more of the GABAergic-related *GAD1* gene ($P<0.01$) and less of the glutamatergic-transporter-encoding *SLC17A7* gene ($P<0.001$) (also known as *VGLUT1*) than hCS (Supplementary Fig. 1j,k).

**Single-cell RNA-sequencing (RNA-seq) of hOLS-derived oligodendrocytes.** To comprehensively characterize oligodendrocyte lineage cells in hOLS, we isolated O4$^+$ cells from day 127 hOLS by immunopanning and performed deep single-cell RNA-sequencing (Fig. 2a). We sequenced 295 cells derived from two hiPS cell lines and compared their profiles to cells isolated from primary human fetal cortex, primary human adult cortex, and hCS[23,24] (Supplementary Fig. 2a). Clustering of all cells using the *t*-distributed stochastic neighbor embedding (*t*-SNE)[25] approach revealed distinct populations of *SOX10*$^+$ oligodendrocytes, *STMN2*$^+$ neurons, *SOX9*$^+$ astrocytes, *CX3CR1*$^+$ microglia, and *FLT1*$^+$ endothelial cells (Fig. 2b,c and Supplementary Fig. 2b). The O4$^+$ cells derived from hOLS clustered most closely to OPCs and mature oligodendrocytes from the primary human adult cortical tissue within the *SOX10*$^+$ cluster (Fig. 2d,e). On closer inspection, the oligodendrocyte cluster contained populations of proliferating cells, OPCs and newly formed oligodendrocytes (NFOs), and myelinating oligodendrocytes derived from hOLS that had similar patterns of marker expression as primary OPCs and primary mature oligodendrocytes (Fig. 2f,g and Supplementary Fig. 2c; also see Supplementary Fig. 3a for examples of genes differentially expressed between primary and hOLS samples). Expression of oligodendrocyte-stage-specific markers was confirmed in cells from each cluster by qPCR (Supplementary Fig. 2d). Moreover, we found O4$^+$ cells in the three oligodendrocyte subclusters in hOLS from two hiPS cell lines and a high transcriptomic consistency across lines (Pearson's $r=0.96$, log normalized gene expression) (Fig. 2h and Supplementary Fig. 2e,f).

To further assess the developmental progression of oligodendrocyte lineage cells in hOLS, we performed Monocle analysis, which utilizes an unsupervised algorithm to reveal single-cell gene expression kinetics over time and orders cells through a biological process[26]. This analysis revealed a spectrum of oligodendrocyte lineage stages in hOLS ranging from dividing cells expressing *MKI67* and *TOP2A*, which closely resemble primary OPCs, to mature cells expressing *MOG* and *MBP*, which closely resemble primary mature oligodendrocytes (Fig. 3a). This analysis further identified several temporal patterns of gene expression, including some genes that were highly expressed early and decreased over pseudotime, some that peaked mid-pseudotime, and others that were more highly expressed at later pseudotime points (Fig. 3b). Early pseudotime genes expressed in dividing oligodendrocytes included *PTPRZ1*, *PDGFRA*, and *CSGP4*; mid-pseudotime genes expressed in immature oligodendrocytes included *SIRT2*, *RASGEF1B*, and *TMEM108;* late pseudotime genes expressed in mature oligodendrocytes included *MOG*, *GSN*, and *MOBP*[27] (Fig. 3c and Supplementary Fig. 3b).

Anticipating that hOLS may be useful for disease modeling, we analyzed the single-cell expression pattern of genes associated with oligodendrocyte-related disorders (Fig. 2e and 3d and Supplementary Fig. 3c). We found that a gene associated with Aicardi–Goutieres syndrome (*RNASEH2A*)[28] was expressed primarily in OPCs and NFOs, and that genes associated with metachromatic leukodystrophy (*ARSA*)[29] and Krabbe disease (*GALC*)[30] were expressed in mature oligodendrocytes. These findings suggest that having access to multiple stages of oligodendrocyte development may be important for disease modeling.

**Maturation of oligodendrocytes in hOLS.** Prompted by the finding that oligodendrocyte lineage cells mature transcriptionally in hOLS, we next examined their morphology and functional properties. During development, bipolar OPCs migrate from their region of origin throughout the cortex where they ultimately cease migrating and extend multiple processes that interact with nearby neurons[31]. To determine whether OPCs migrate in hOLS as they do in vivo, we used temperature-controlled live imaging with a previously described *Sox10*-MCS5::eGFP reporter[32] at in vitro differentiation stages ranging from day 65 up to day 275 in culture (Fig. 4a). We found that the propensity of *Sox10*-MCS5::eGFP$^+$ cells to migrate peaked between days 110 and 180 of in vitro culture, but all *Sox10*-MCS5::eGFP$^+$ cells were stationary by day 235 (Fig. 4b; $n=5$–8 hOLS from 5 hiPS cell lines; $P<0.01$).

We next sought to determine whether hOLS-derived oligodendrocyte lineage cells mature electrophysiologically. As OPCs mature to multipolar oligodendrocytes, expression of voltage-gated sodium and potassium channels is progressively reduced[33,34]. We performed whole cell current clamp recordings from bipolar and multipolar

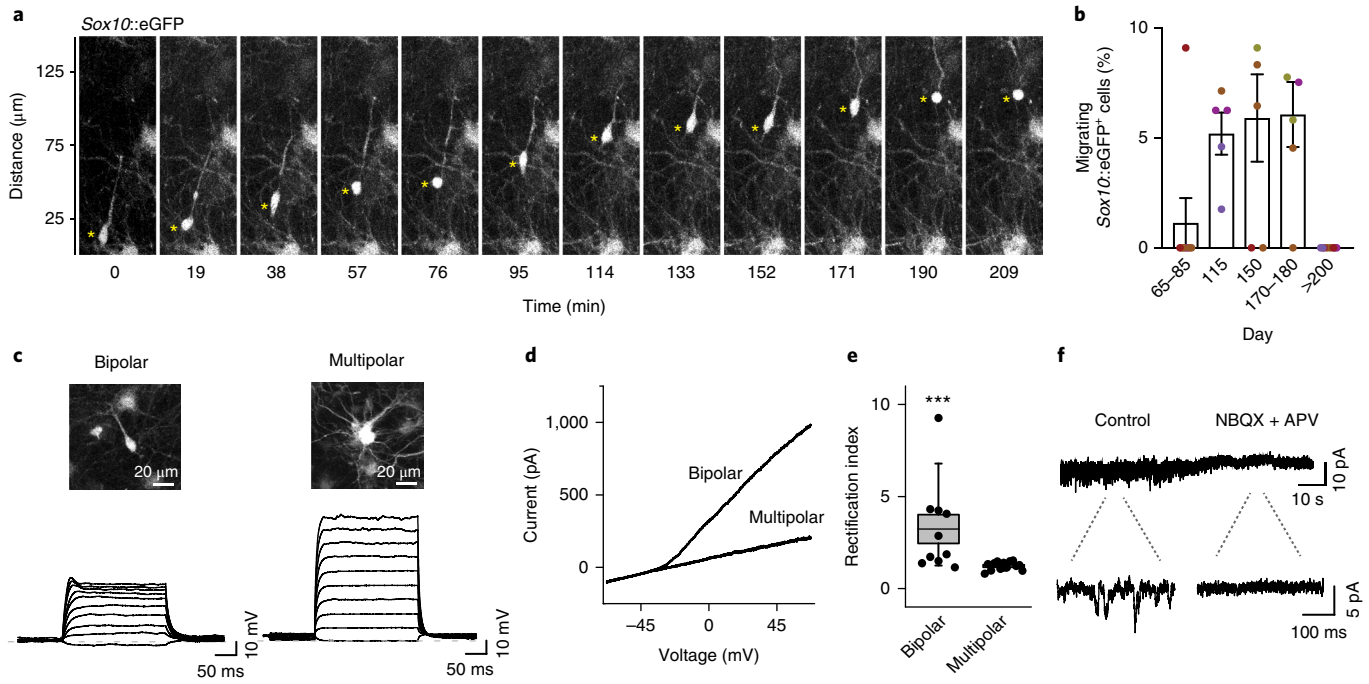


**Fig. 4 | Oligodendrocyte maturation in hOLS. a**, Example of time lapse imaging of a migrating *Sox10*-MCS5::eGFP+ cell in hOLS. **b**, Percentage of migrating *Sox10*-MCS5::eGFP+ cells over differentiation time in vitro (days 65–85: $n=8$ hOLS from 3 hiPS cell lines; day 115: $n=5$ hOLS from 3 hiPS cell lines; day 150: $n=6$ hOLS from 3 hiPS cell lines; days 170–180: $n=6$ hOLS from 3 hiPS cell lines; day >200: $n=8$ hOLS from 4 hiPS cell lines; see Supplementary Table 1). Lines are shown in different colors; asterisk indicates the soma of a migrating cell; Kruskal–Wallis test, $P=0.003$. Data are mean ± s.e.m. **c**, Slice recordings in hOLS showing membrane voltage responses in bipolar and multipolar cells following intracellular current injections. **d**, Example of an I-V curve showing an outward rectifying current in a bipolar cell but not in a multipolar cell. For **c** and **d**, recordings were repeated in 12 bipolar cells and 13 multipolar cells from 3 independent inductions with similar results. **e**, Quantification of the rectification index in bipolar and multipolar *Sox10*-MCS5::eGFP+ cells ($n=13$ multipolar cells, $n=12$ bipolar cells, two-tailed Mann–Whitney test, ***$P=0.0009$). Dots represent individual cells, box edges represent s.e.m., the middle horizontal lines within the box represent the mean, and whiskers represent the 10th and 90th percentiles of the population. **f**, Voltage clamp recording from a representative bipolar *Sox10*-MCS5::eGFP+ cell showing a reduction in holding current variance in response to the blockers of glutamate receptors APV (40 μM) and NBQX (20 μM). Recordings were repeated in five cells from two independent inductions with similar results.

*Sox10*-MCS5::eGFP+ cells in slices of hOLS from days 108 to 175 (Fig. 4c). We observed that the membrane response to current injection of bipolar cells, but not multipolar cells, was highly nonlinear, indicating expression of voltage-dependent sodium and potassium channels in the former. In fact, the I-V curve of bipolar-shaped cells showed outwardly rectifying currents suggestive of slowly inactivating potassium currents (Fig. 4d,e; $n=10$–13 cells, $P<0.001$), and this difference was accompanied by complementary differences in input resistance and capacitance (Supplementary Fig. 4a, b). Moreover, during oligodendrocyte development, the release of glutamate by nearby neurons plays an instructive role in OPC differentiation[35,36]. We tested for sensitivity to released glutamate in voltage-clamped *Sox10*-MCS5::eGFP+ cells and observed discrete inward-going events in approximately 70% of bipolar and multipolar cells ($n=13$ and 10 cells, respectively; Fig. 4f). These events were blocked by application of 40 μM APV and 20 μM NBQX ($n=5$ cells; Fig. 4f and Supplementary Fig. 4c), indicating that *Sox10*-MCS5::eGFP+ cells express ionotropic glutamate receptors that are spontaneously activated in hOLS.

A hallmark of oligodendrocyte maturation is the ability to interact with and myelinate neuronal axons. We immunostained hOLS cryosections at day 115 for MBP and NF-H and observed the interaction of oligodendrocyte processes and nearby axons (Fig. 5a). Moreover, in hOLS cryosections obtained at day 150–158, we identified examples of MBP flanking neurofilament staining, indicative of myelination (Fig. 5b,c and Supplementary Fig. 4d). We found that, at days 150–160, ~28% of MBP+ cells interacted with NF-H+ processes (Fig. 5d; $n=9$ hOLS from 3 hiPS cell lines). To verify myelination, we performed transmission electron microscopy at days 100–170 in hOLS derived from three hiPS cell lines and found various stages of myelination, including lamellae of compact myelin surrounding axons (Fig. 5e,f and Supplementary Fig. 4e,f). Lastly, as a proof of principle that hOLS can be used to study oligodendrocyte loss or injury, we treated day 75–85 hOLS with the toxic phospholipid lysolecithin for 15–17 h (Fig. 5g), which has been shown to cause demyelination in vivo and in explant cultures[37–39]. Monitoring by live imaging at 4–6 h after treatment revealed changes in the morphology and loss of *Sox10*-MCS5::eGFP+ cells (Fig. 5g,h).

## Discussion

We demonstrate the generation of human oligodendrocyte lineage cells in a 3D cellular platform that includes multiple stages of oligodendrocyte development, migration, and myelination. Our system produces neurons and astrocytes that spatially and temporally overlap with oligodendrocytes, allowing interaction between cell types. This model has several advantages over existing methods to produce oligodendrocytes in vitro, including the existence of multiple mature cell types (Supplementary Table 2). In addition, the 3D nature of this platform more closely resembles the cytoarchitecture and cellular milieu that oligodendrocytes would encounter in vivo. There is increasing evidence of the importance of interactions between oligodendrocytes and astrocytes and between oligodendrocytes and neurons during development both through secreted factors and physical interactions[5,8–11], and the recapitulation of these interactions may be essential to building more realistic in vitro models of brain function and dysfunction.

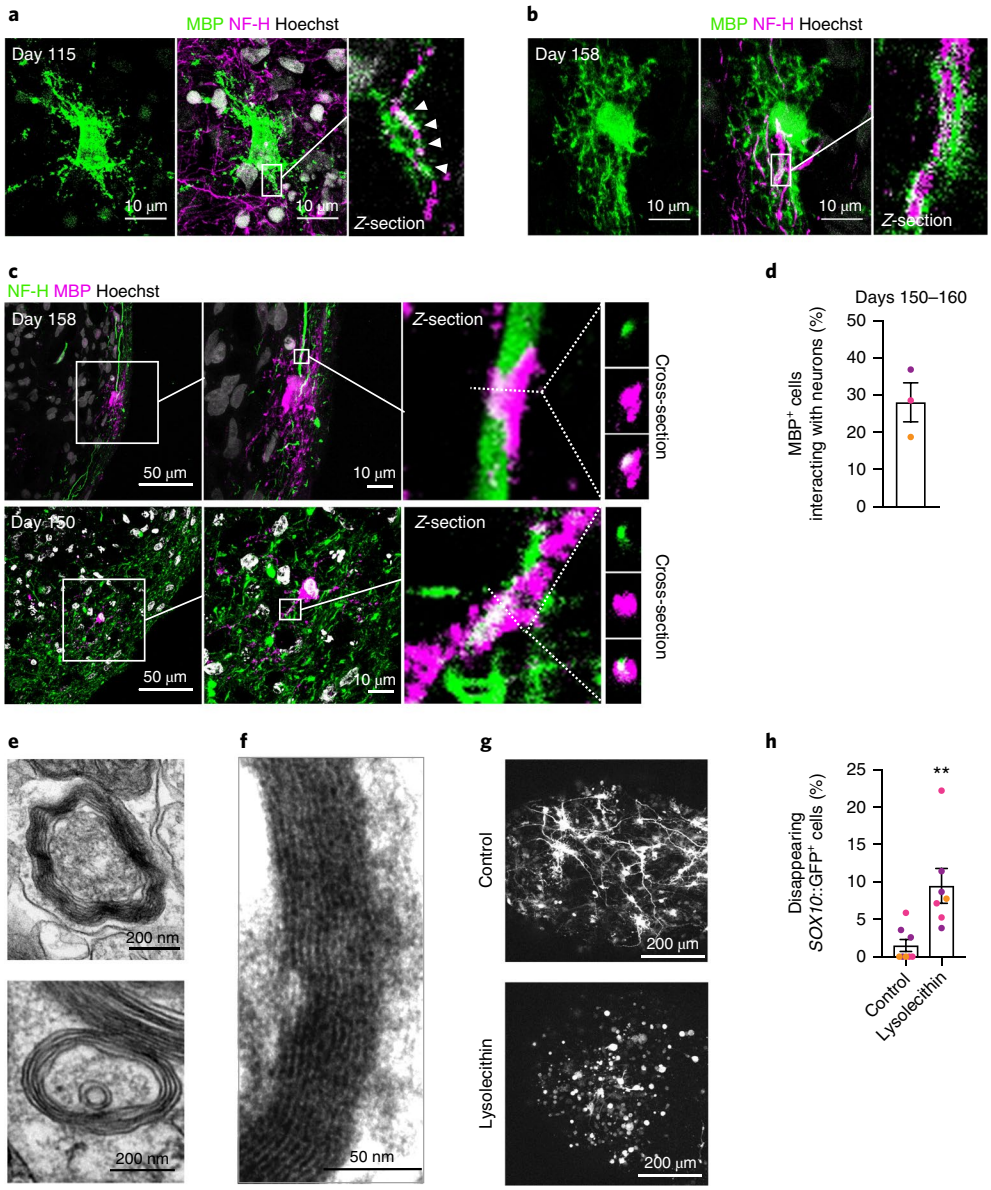


**Fig. 5 | Oligodendrocyte–neuron interaction and myelination in hOLS. a**,**b**, Immunostaining of hOLS cryosections with MBP and NF-H ($n = 9$ hOLS from 3 hiPS cell lines). **c**, Example images of interactions between MBP$^+$ cells and NF-H$^+$ processes in cryosections at days 150–158 of in vitro culture imaged by confocal microscopy. The first and seconds panels of each row are maximum projections, the third panel of each row is an individual *z*-section, and the right most panels are cross-sections. **d**, Quantification of MBP$^+$ cells that interact with NF-H$^+$ neurons out of total MBP$^+$ cells. **e**,**f**, Transmission electron microscopy images of hOLS at day 103 of differentiation showing myelin in line 2242-1. Examples from hOLS derived from other hiPS cell lines are shown in Supplementary Fig. 4. Electron microscopy was performed on hOLS from three independent inductions with similar results. **g**, Example images of *Sox10*-MCS5::eGFP$^+$ cells in untreated and lysolecithin-treated hOLS after 13 h of live imaging. **h**, Percentage of *Sox10*-MCS5::eGFP$^+$ cells that disappear during the 13-h live imaging experiment following lysolecithin treatment ($n = 8$ untreated hOLS from 3 hiPS cell lines, $n = 7$ lysolecithin-treated hOLS from 3 hiPS cell lines, two-tailed Mann–Whitney test, $^{**}P = 0.001$). Data are mean ± s.e.m. Scale bars, 200 µm (**g**), 50 µm (**c** left panel), 10 µm (**a, b, c** middle panel), 200 nm (**e**), and 50 nm (**f**).

To validate the stages of oligodendrocyte development in hOLS, we performed deep single-cell RNA-seq and identified a progression of oligodendrocyte lineage cells from dividing progenitors to mature oligodendrocytes. We additionally compared these transcriptional data to the signature of primary human oligodendrocytes isolated from human cerebral cortex and found that they clustered closely. Future studies are necessary to confirm transcriptional similarity in additional hiPS cell lines and with larger cell numbers.

The transcriptional maturation of oligodendrocyte lineage cells in hOLS was accompanied by functional changes as assessed by electrophysiology and electron microscopy. The maturation and similarity of oligodendrocytes in hOLS to primary adult samples suggest that this model can be applied to answer basic questions regarding human oligodendrocyte development, as demonstrated by the expression of white-matter-disease-related genes in single cells derived from hOLS. To study later stages of oligodendrocyte maturation and myelination, future methods need to be developed to better quantify the extent of compact myelination in 3D culture. Quantifying wrapping by traditional electron microscopy techniques is difficult as a result of inconsistency in the directionality of axons in

hOLS. However, these current limitations may be resolved by incorporating scaffolds to guide projecting axons in hOLS or by performing high-throughput electron microscopy to image larger areas of hOLS and obtain more accurate quantifications of myelination.

A remaining obstacle in the use of 3D cultures to study disease processes is the inherent inter- and intra-organoid variability that complicates the comparison between control and disease-related cultures[40]. Strategies to limit the variability between organoids include directing differentiation to specific brain regions, limiting the use of embedding in extracellular matrices that can induce spurious fates, using cell-specific reporters for imaging cell types of interest, and using single cell sequencing[19,41]. In hOLS, the variability in OPC yield is higher at earlier stages and decreases over time. Notably, we also found that transcriptional variability is lower at later stages of hCS differentiation[42]. This suggests that, for future applications, allowing hOLS to mature to around day 100 would result in higher consistency.

This hOLS method can be used to live image multiple stages of oligodendrocyte development over long periods of time in vitro to dissect the physical mechanisms of OPC migration and myelination. Here, as a proof of principle, we demonstrate that treatment with lysolecithin induces oligodendrocyte cell loss and that this process can be monitored by live imaging. Future studies can apply this cellular model to study leukodystrophies and other disorders affecting myelination in the CNS. The hOLS have the potential to be fused with other brain region-specific spheroids to derive brain assembloids[19,21] to study the migration and differentiation of oligodendrocyte lineage cells in different brain regions. hOLS may also potentially be combined with autologous patient-derived immune cells to study neuro-immune dysfunction, such as in multiple sclerosis. The personalized nature of the hiPS-cell-derived platform will further allow the study of these cellular processes in the context of disease, such as vanishing white matter disorder[12], or environmental alterations, such as the effect of hypoxic injury on the premature brain[43]. The scalability of hOLS also makes this system amenable to genetic and small molecule screens to discover modulators of human myelination and identify novel therapeutics.

## Online content

Any methods, additional references, Nature Research reporting summaries, source data, statements of data availability and associated accession codes are available at https://doi.org/10.1038/s41593-018-0316-9.

Received: 13 June 2018; Accepted: 5 December 2018;
Published online: 28 January 2019

## References

1. Nave, K. A. Myelination and the trophic support of long axons. *Nat. Rev. Neurosci.* **11**, 275–283 (2010).
2. Menichella, D. M. et al. Genetic and physiological evidence that oligodendrocyte gap junctions contribute to spatial buffering of potassium released during neuronal activity. *J. Neurosci.* **26**, 10984–10991 (2006).
3. Fünfschilling, U. et al. Glycolytic oligodendrocytes maintain myelin and long-term axonal integrity. *Nature* **485**, 517–521 (2012).
4. Dai, X. et al. The trophic role of oligodendrocytes in the basal forebrain. *J. Neurosci.* **23**, 5846–5853 (2003).
5. Orthmann-Murphy, J. L., Freidin, M., Fischer, E., Scherer, S. S. & Abrams, C. K. Two distinct heterotypic channels mediate gap junction coupling between astrocyte and oligodendrocyte connexins. *J. Neurosci.* **27**, 13949–13957 (2007).
6. Moore, C. S., Abdullah, S. L., Brown, A., Arulpragasam, A. & Crocker, S. J. How factors secreted from astrocytes impact myelin repair. *J. Neurosci. Res.* **89**, 13–21 (2011).
7. Simons, M. & Trajkovic, K. Neuron-glia communication in the control of oligodendrocyte function and myelin biogenesis. *J. Cell Sci.* **119**, 4381–4389 (2006).
8. Barres, B. A., Schmid, R., Sendnter, M. & Raff, M. C. Multiple extracellular signals are required for long-term oligodendrocyte survival. *Development* **118**, 283–295 (1993).
9. Lin, S. C. & Bergles, D. E. Synaptic signaling between GABAergic interneurons and oligodendrocyte precursor cells in the hippocampus. *Nat. Neurosci.* **7**, 24–32 (2004).
10. Bergles, D. E., Roberts, J. D., Somogyi, P. & Jahr, C. E. Glutamatergic synapses on oligodendrocyte precursor cells in the hippocampus. *Nature* **405**, 187–191 (2000).
11. Hardy, R. & Reynolds, R. Neuron-oligodendroglial interactions during central nervous system development. *J. Neurosci. Res.* **36**, 121–126 (1993).
12. van der Knaap, M. S., Pronk, J. C. & Scheper, G. C. Vanishing white matter disease. *Lancet Neurol.* **5**, 413–423 (2006).
13. Wolswijk, G. Oligodendrocyte survival, loss and birth in lesions of chronic-stage multiple sclerosis. *Brain* **123**, 105–115 (2000).
14. Douvaras, P. & Fossati, V. Generation and isolation of oligodendrocyte progenitor cells from human pluripotent stem cells. *Nat. Protoc.* **10**, 1143–1154 (2015).
15. Numasawa-Kuroiwa, Y. et al. Involvement of ER stress in dysmyelination of Pelizaeus–Merzbacher disease with PLP1 missense mutations shown by iPSC-derived oligodendrocytes. *Stem Cell Rep.* **2**, 648–661 (2014).
16. Stacpoole, S. R. et al. High yields of oligodendrocyte lineage cells from human embryonic stem cells at physiological oxygen tensions for evaluation of translational biology. *Stem Cell Rep.* **1**, 437–450 (2013).
17. Wang, S. et al. Human iPSC-derived oligodendrocyte progenitor cells can myelinate and rescue a mouse model of congenital hypomyelination. *Cell Stem Cell* **12**, 252–264 (2013).
18. Hogberg, H. T. et al. Toward a 3D model of human brain development for studying gene/environment interactions. *Stem Cell Res. Ther.* **4**(Suppl 1), S4 (2013).
19. Pașca, S. P. The rise of three-dimensional human brain cultures. *Nature* **553**, 437–445 (2018).
20. Pașca, A. M. et al. Functional cortical neurons and astrocytes from human pluripotent stem cells in 3D culture. *Nat. Methods* **12**, 671–678 (2015).
21. Birey, F. et al. Assembly of functionally integrated human forebrain spheroids. *Nature* **545**, 54–59 (2017).
22. Sloan, S. A., Andersen, J., Pașca, A. M., Birey, F. & Pașca, S. P. Generation and assembly of human brain region-specific three-dimensional cultures. *Nat. Protoc.* **13**, 2062–2085 (2018).
23. Darmanis, S. et al. A survey of human brain transcriptome diversity at the single cell level. *Proc. Natl Acad. Sci. USA* **112**, 7285–7290 (2015).
24. Sloan, S. A. et al. Human astrocyte maturation captured in 3D cerebral cortical spheroids derived from pluripotent stem cells. *Neuron* **95**, 779–790.e6 (2017).
25. van der Maaten, L. & Hinton, G. Visualizing data using t-SNE. *J. Mach. Learn. Res.* **9**, 2579–2605 (2008).
26. Trapnell, C. et al. The dynamics and regulators of cell fate decisions are revealed by pseudotemporal ordering of single cells. *Nat. Biotechnol.* **32**, 381–386 (2014).
27. Zhang, Y. et al. Purification and characterization of progenitor and mature human astrocytes reveals transcriptional and functional differences with mouse. *Neuron* **89**, 37–53 (2016).
28. Crow, Y. J. et al. Mutations in genes encoding ribonuclease H2 subunits cause Aicardi–Goutières syndrome and mimic congenital viral brain infection. *Nat. Genet.* **38**, 910–916 (2006).
29. Gomez-Ospina, N. Arylsulfatase A deficiency. in *GeneReviews* (eds. Adam, M. P. et al.) (Univ. Washington, Seattle, 2006).
30. Austin, J. et al. Studies in globoid (Krabbe) leukodystrophy (GLD). V. Controlled enzymic studies in ten human cases. *Arch. Neurol.* **23**, 502–512 (1970).
31. Bergles, D. E. & Richardson, W. D. Oligodendrocyte development and plasticity. *Cold Spring Harb. Perspect. Biol.* **8**, a020453 (2015).
32. Pol, S. U. et al. Sox10-MCS5 enhancer dynamically tracks human oligodendrocyte progenitor fate. *Exp. Neurol.* **247**, 694–702 (2013).
33. Sontheimer, H., Trotter, J., Schachner, M. & Kettenmann, H. Channel expression correlates with differentiation stage during the development of oligodendrocytes from their precursor cells in culture. *Neuron* **2**, 1135–1145 (1989).
34. Livesey, M. R. et al. Maturation and electrophysiological properties of human pluripotent stem cell-derived oligodendrocytes. *Stem Cells* **34**, 1040–1053 (2016).
35. Káradóttir, R. & Attwell, D. Neurotransmitter receptors in the life and death of oligodendrocytes. *Neuroscience* **145**, 1426–1438 (2007).
36. Káradóttir, R., Cavelier, P., Bergersen, L. H. & Attwell, D. NMDA receptors are expressed in oligodendrocytes and activated in ischaemia. *Nature* **438**, 1162–1166 (2005).
37. Birgbauer, E., Rao, T. S. & Webb, M. Lysolecithin induces demyelination in vitro in a cerebellar slice culture system. *J. Neurosci. Res.* **78**, 157–166 (2004).
38. Blakemore, W. F., Eames, R. A., Smith, K. J. & McDonald, W. I. Remyelination in the spinal cord of the cat following intraspinal injections of lysolecithin. *J. Neurol. Sci.* **33**, 31–43 (1977).

39. Hall, S. M. The effect of injections of lysophosphatidyl choline into white matter of the adult mouse spinal cord. *J. Cell Sci.* **10**, 535–546 (1972).
40. Amin, N. D. & Paşca, S. P. Building models of brain disorders with three-dimensional organoids. *Neuron* **100**, 389–405 (2018).
41. Di Lullo, E. & Kriegstein, A. R. The use of brain organoids to investigate neural development and disease. *Nat. Rev. Neurosci.* **18**, 573–584 (2017).
42. Yoon, S. et al. Reliability of human cortical organoid generation. *Nat. Methods* **16**, 75–78 (2019).
43. Volpe, J. J. The encephalopathy of prematurity – brain injury and impaired brain development inextricably intertwined. *Semin. Pediatr. Neurol.* **16**, 167–178 (2009).

## Acknowledgements

This paper is dedicated to the memory of our wonderful colleague and mentor Ben A. Barres. We thank B.A. Barres, B. Zuchero, and members of the Pasca laboratory for scientific input, J. Perrino (Stanford Cell Sciences Imaging Facility) for support with electron microscopy, as well as F. Sim (University of Buffalo) for providing the *Sox10-MCS5*::eGFP plasmid. This work was supported by the US National Institutes of Health BRAINS Award (MH107800), the MQ Fellow Award, the NYSCF Robertson Stem Cell Investigator Award, the Stanford Wu Tsai Neurosciences Institute's Brain Rejuvenation Project and the Human Brain Organogenesis Project, the Kwan Research Fund and the California Institute of Regenerative Medicine, the Child Health Research Institute Pilot Award, and the NARSAD Independent Investigator Award from the Brain and Behavior Research Foundation (to S.P.P.); the National Science Foundation Graduate Research Fellowship and the Bio-X Stanford Interdisciplinary Graduate Fellowship (to R.M.M.); Stanford Medicine's Dean's Fellowship (to Y.M.); and NIMH T32GM007365, F30MH106261, and Bio-X Predoctoral Fellowship (to or supporting S.A.S.).

## Author contributions

R.M.M. performed the differentiation experiments. Q.L. carried out single-cell library preparations and S.A.S. analyzed single-cell data. O.R. and J.R.H. conducted and analyzed electrophysiological experiments. R.M.M., Y.M., and R.J.L. carried out all other experiments and data analyses. R.M.M. and S.P.P. conceived the project, designed experiments, and wrote the manuscript with input from all authors. S.P.P. supervised the work.

## Competing interests

Stanford University has filed a provisional patent application that covers the generation of myelinating oligospheroids for studying human development and disease (US patent application number 15/953,197).

## Additional information

**Supplementary information** is available for this paper at https://doi.org/10.1038/s41593-018-0316-9.

**Reprints and permissions information** is available at www.nature.com/reprints.

**Correspondence and requests for materials** should be addressed to S.P.P.

**Publisher's note:** Springer Nature remains neutral with regard to jurisdictional claims in published maps and institutional affiliations.

## Methods

**Culture of hiPS cells.** The hiPS cell lines used in this study were validated using standardized methods as previously described[44,45]. Cultures were tested for and maintained mycoplasma free. A total of seven control hiPS cell lines derived from fibroblasts collected from seven subjects were used for experiments (Supplementary Table 1). The hiPS cell line H20961 was derived by the Gilad laboratory[46]. Approval for hiPS cell work was obtained from the Stanford Institutional Review Board panel and informed consent was obtained from all subjects.

**Generation of hCS and hOLS from hiPS cells.** hiPS cells were cultured on vitronectin-coated plates (5 μg ml$^{-1}$, Thermo Fisher, A14700) in Essential 8 medium (Thermo Fisher, A1517001). Cells were passaged every 4 d with 0.5 mM EDTA (Life Technologies, pH 8.0).

For the generation of 3D neural spheroids, hiPS cells were incubated with accutase (Innovate Cell Technologies, AT104) at 37°C for 7 min and dissociated into single cells. To obtain uniformly sized spheroids, AggreWell-800 (Stemcell Technologies, 34815) containing 300 microwells was used. Approximately $3\times10^6$ single cells were added per AggreWell-800 well in Essential 8 medium supplemented with the ROCK inhibitor Y-27632 (10 μM, EMD Chemicals, S1049), centrifuged to capture the cells in the microwells, and incubated at 37°C with 5% $CO_2$. After 18–24 h, spheroids consisting of approximately 10,000 cells were collected from each microwell by pipetting medium in the well up and down with a cut pipet tip and transferred into ultra-low attachment plastic dishes (Thermo Fisher, 3262) in Essential 6 medium (Thermo Fisher, A1516401) supplemented with two SMAD pathway inhibitors—dorsomorphin (2.5 μM, Sigma-Aldrich, P5499-CONF) and SB-431542 (10 μM, R&D Systems, 1614). For the first 5 d, Essential 6 medium was changed every day and supplemented with dorsomorphin and SB-431542.

To generate hOLS, on day 6 in suspension the spheroids were transferred to differentiation and maintenance medium (DMM) containing DMEM/F12 (Thermo Fisher, 11330-057), B-27 supplement without vitamin A (Thermo Fisher, 12587010), N2 supplement (Thermo Fisher, 17502048), minimum essential media (MEM) non-essential amino acids (1:100, Thermo Fisher, 11140076), GlutaMax (1:100, Thermo Fisher, 35050079), human insulin (25 μg ml$^{-1}$, Sigma-Aldrich, I9278-5ML), β-mercaptoethanol (0.1 mM; Sigma-Aldrich M3148), and penicillin-streptomycin (1:100, Thermo Fisher, 15140163). The DMM was supplemented with 20 ng ml$^{-1}$ EGF (R&D Systems, 236-EG-01M) and 20 ng ml$^{-1}$ basic fibroblast growth factor (bFGF) (Peprotech, 100-26) for 19 d (until day 24) with daily medium change in the first 10 d, and every other day for the subsequent 9 d. The Wnt pathway inhibitor IWP-2 (5 μM, Selleckchem, S7085) was added from day 4 until day 24, and the small molecule SHH pathway smoothened agonist (1 μM, Millipore Sigma, 566660) was added from day 12 to day 24. From day 25 to day 36, hOLS were cultured in DMM supplemented with T3 (60 ng ml$^{-1}$, Sigma-Aldrich, T2877), biotin (100 ng ml$^{-1}$, Sigma-Aldrich, B4639), NT-3 (20 ng ml$^{-1}$, Peprotech, 450-03), BDNF (20 ng ml$^{-1}$, Peprotech, 450-02), cAMP (1 μM, Sigma-Aldrich, D0627), hepatocyte growth factor (5 ng ml$^{-1}$, Peprotech, 315-23), insulin-like growth factor 1 (10 ng ml$^{-1}$, VWR, 100-11), and PDGF-AA (10 ng ml$^{-1}$, R&D Systems, 221-AA). From day 37 onwards, hOLS were cultured in complete DMM (DMM supplemented with T3, biotin, cAMP, and ascorbic acid; 20 μg ml$^{-1}$, Wako Pure Chemical, 323-44822). From day 17 to day 43, media changes were performed every other day. From day 44 onwards, media changes were preformed every 4–5 d.

The generation of hCS from hiPS cells was performed similarly to a method we previously described[20]. To generate hCS, on day 6 in suspension the microwell-generated spheroids were transferred to neural medium containing Neurobasal A (Thermo Fisher, 10888022), B-27 supplement without vitamin A (Life Technologies, 12587), GlutaMax (Life Technologies, 1:100), and penicillin-streptomycin (1:100, Thermo Fisher, 15140163). Neural medium was supplemented with 20 ng ml$^{-1}$ EGF (R&D Systems) and 20 ng ml$^{-1}$ bFGF (R&D Systems) for 19 d (until day 24) with daily medium change in the first 10 d, and every other day for the subsequent 9 d. To promote differentiation of the neural progenitors into neurons, neural medium was supplemented with 20 ng ml$^{-1}$ BDNF (Peprotech, 450-02) and 20 ng ml$^{-1}$ NT-3 (Peprotech, 450-03) with medium changes every other day. From day 44, only neural medium without growth factors was used for medium changes every 4 d.

**Cryopreservation.** hOLS were fixed in 4% paraformaldehyde (PFA) overnight. They were then washed in PBS and transferred to 30% sucrose for 3–7 d. Subsequently, they were rinsed in optimal cutting temperature (OCT) and 30% sucrose (1:1) and embedded in OCT (Tissue-Tek OCT Compound 4583, Sakura Finetek) and stored at −80 °C. For immunofluorescence, 12–14-μm-thick sections were cut using a Leica cryostat.

**Immunofluorescence.** Cryosections were washed with PBS to remove excess OCT and blocked in 10% normal donkey serum (NDS, Abcam, AB7475), 0.3% Triton X-100 (Sigma-Aldrich, X-100) diluted in PBS for 1 h at room temperature. The sections were then incubated overnight at 4 °C with primary antibodies diluted in PBS containing 10% NDS and 0.3% Triton X-100. PBS was used to wash off the primary antibodies and the cryosections were incubated with secondary antibodies in PBS with 10% NDS and 0.3% Triton X-100 for 1 h. Dissociated cultures on glass coverslips were fixed in 4% PFA in PBS for 15 min at 4 °C and then rinsed for 5 min with PBS. The coverslips were then treated with 0.1% Triton X-100 in PBS for 15 min at room temperature except for when staining for PDGFRα. The coverslips were blocked for 1 h at room temperature with 5% NDS in PBS and then incubated overnight at 4 °C with primary antibodies diluted in PBS containing 5% NDS. PBS was used to wash off the primary antibodies and the cryosections were incubated with secondary antibodies in PBS with 5% NDS for 1 h. The following primary antibodies were used for immunofluorescence: anti-OLIG2[47] (rabbit, 1:500, Millipore, AB9610), anti-NKX2-2[48] (mouse, 1:200, DSHB, 74.5A5), anti-PDGFRα[49] (rabbit, 1:500, Santa Cruz, sc-338), anti-O4[50] (mouse, 1:500, R&D Systems, MAB1326), anti-O1[51] (mouse, 1:200, R&D Systems, MAB1327), anti-MBP[52] (rat, 1:300, Millipore, MAB386), anti-GFAP[53] (rabbit, 1:1,000, Agilent DAKO, Z0334), anti-Neurofilament-H 200K[54] (mouse, 1:500, Abcam, AB7795), anti-GABA[55] (rabbit, 1:1,000, Sigma, A2052), and anti-MAP2[56] (guinea pig, 1:2,500 on coverslips, 1:10,000 on cryosections, Synaptic Systems, 188004). Alexa Fluor dyes (Life Technologies) were used at 1:1,000 dilution on cryosections and 1:2,000 on coverslips for amplification of the signal. Nuclei were visualized with Hoechst 33258 (Life Technologies, H3549). Cryosections were mounted for microscopy on glass slides using Aquamount (Polysciences, 18606) and imaged on a Zeiss M1 Axioscope, Leica TCS SP8 confocal microscope, or Keyence BZ-X710. Images were processed in ImageJ (Fiji Version 2.0.0). For the analysis in Fig. 5d, the proportion of MBP$^+$ cells overlapping for more than 1 μm with NF-H in 0.5-μm *z*-sections was counted.

**Dissociation and immunopanning of hOLS.** For the enzymatic dissociation of hOLS for culture in monolayer and immunocytochemistry, hOLS were incubated with accutase for 30 min at 37 °C, washed with 10% fetal bovine serum (FBS) (Thermo Fisher, 16000-044) in Hank's balanced salt solution (HBSS) (Thermo Fisher, 14180046), and gently triturated using a P200 pipette. Cells were centrifuged and resuspended in complete DMM. The cells were plated on glass coverslips (15 mm, Warner Instruments, 640713) coated with poly-L-ornithine (50 μg ml$^{-1}$, Sigma-Aldrich, P3655) and laminin (5 μg ml$^{-1}$, Sigma-Aldrich, L2020) at a density of around 1 spheroid per 2 coverslips.

To dissociate and isolate O4$^+$ cells from hOLS for single cell profiling, we adapted a previously published protocol used for primary human fetal brain tissue[27]. Plastic Petri plates (10-cm, Thomas Scientific, 351058) were coated with 20 μl anti-mouse IgG (Thermo Fisher, A-21042) in 7 ml 50 mM Tris-HCl pH9.5 (Fisher Scientific, T1095) at 4 °C overnight. The following day, each plate was rinsed 3 times with PBS and then coated with 1.78 μl anti-O4 hybridoma (obtained from the B.A. Barres laboratory at Stanford University[27]) in 2.55 ml 0.02% BSA diluted in PBS (Caisson Labs, PBL02) at room temperature for at least 3 h and rinsed 4–5 times with PBS before use. Up to 6 spheroids per immunopanning plate were dissociated with accutase as described above and resuspended in 10 ml 0.02% BSA. The resulting suspension was added to a precoated plastic Petri culture dish for at least 40 min with gentle occasional swirling. The supernatant was then removed from the O4-treated plates and the plates were rinsed with PBS 6–8 times to remove unattached cells. O4$^+$ cells were detached from the plates using 0.25% trypsin (Thermo Fisher, 25200056) for 5 min at 37 °C. Cells were washed in DMEM (Thermo Fisher, 10313-039) containing FBS and centrifuged for 5 min at 1,200 r.p.m., and resuspended in 0.02% BSA and supplemented with Y-27632 (10 μM, EMD Chemicals, S1049). The suspension was filtered through a 40-μm strainer (Fisher Scientific, 352340) and single cells were sorted into lysis buffer, 4 μl each in 96-well plates (Bio-Rad, HSP9631). The lysis buffer contains 4 enzyme units (U) of RNase inhibitor (40 U μl$^{-1}$, Clontech, 2313B), 0.05% Triton, 2.5 mM deoxynucleotide triphosphates (dNTP), 2.5 μM Oligo-d$T_{30}$VN (IDT, RNase-free HPLC purification)[57], external RNA control consortium (ERCC) RNA Spike-In Mix (1:2.4 × 10$^7$ diluted, Thermo Fisher, 4456740). Plates were briefly vortexed and spun down before being stored in a −80 °C freezer until downstream processing.

**Single cell RNA-seq library preparation.** Sorted cells ($n = 332$) in 96-well plates were thawed on ice and immediately used for library preparation following the Smartseq2 protocol[57] with modifications. Briefly, plates were incubated at 72 °C for 3 min, during which RNA molecules with polyA tails were annealed with Oligo-d$T_{30}$VN, and then they were immediately chilled on ice. Reverse transcription mixture was added at 6 μl per well so that the final solution contained 95 enzyme units (U) SMARTScribe Reverse Transcriptase (100 U μl$^{-1}$, Clontech, 639538), 10 enzyme units (U) RNase inhibitor (40 U μl$^{-1}$), 1 × First-Strand buffer, 5 mM dithiothreitol, 1 M betaine, 6 mM $MgCl_2$, 1 μM template switching oligos (TSO) (Exiqon, RNase-free HPLC purification)[57]. Reverse transcription was performed at 42 °C for 90 min, followed by 70 °C, 5 min. To amplify the whole transcriptome, 15 μl DNA amplification mixture was added with the final solution containing 1 × KAPA HIFI Hotstart Master Mix (Kapa Biosciences, KK2602), 0.1 μM in situ polymerase chain reaction (ISPCR) oligo[57], and 0.56U lambda exonuclease (5 U μl$^{-1}$, New England BioLabs, M0262S). cDNA was amplified using (1) 37 °C 30 min; (2) 95 °C 3 min; (3) 21 cycles of 98 °C 20 s, 67 °C 15 s, 72 °C 4 min; and (4) 72 °C 5 min. Amplified cDNA was then purified using PCRClean DX beads (~0.7 volume, Aline Biosciences, C-1003-50), and reconstituted in 20 μl elution buffer (EB). The cDNA quality and quantity were assessed using a fragment analyzer (AATI, High Sensitivity NGS Fragment Analysis Kit: 1–6,000 base pairs (bp)), and samples with

concentrations below 0.08 ng µl$^{-1}$ or abnormal peak patterns were filtered out. A total of 295 cDNA samples (retaining 88.9% of initially sorted) were diluted down to 0.15 ng µl$^{-1}$ (only if above it) and pooled into a 384-well plate using a Mosquito X1 (TTP Labtech). Library preparation was performed using Nextera XT DNA Sample Prep Kit (Illumina, FC-131-1096) and Nextera XT 384 dual index primers, with the help of a Mosquito HTS machine for liquid transfer. For the tagmentation step, 0.4 µl cDNA (30–60 pg), 0.4 µl Tagment Enzyme, and 0.8 µl Tagment DNA Buffer were mixed and incubated at 55 °C for 10 min, followed by neutralization (0.4 µl Neutralize Tagment Buffer). Indexes (0.5 µM each) were added along with Nextera PCR Master Mix to a final volume of 4 µl in each well. PCR was performed as follows: (1) 72 °C 3 min; (2) 95 °C 30 s; (3) 10 cycles of 95 °C 10 s, 55 °C 30 s, 72 °C 1 min; and (4) 72 °C 5 min. All samples were pooled (0.5 µl each) together into a 1.5-ml Eppendorf tube, and the mixed libraries were purified twice with PCRClean DX beads (~0.7 volume each time). The final sample was reconstituted in 50 µl EB buffer, and the concentration and peaks were measured by Qubit and Bioanalyzer.

**Single-cell RNA-sequencing and quality control.** In total, 332 single cells using 101-bp paired end reads were sequenced on a HiSeq 4000 (Illumina). Raw reads were preprocessed and aligned to the human genome (hg38) using the pipeline described in ref. [23], which includes Spliced Transcripts Alignment to a Reference (STAR) alignment and feature counts. As a quality metric, we first performed hierarchical clustering on all cells using a list of housekeeping genes and removed any cells with uniformly low expression across all genes. We separated the resulting dendrogram into two clusters containing cells that passed or failed this quality control. All downstream analyses were performed using only the 295 cells that passed quality control. After quality control and mapping, there was an average of 509,376 mapped reads per cell. These 295 cells were added to data from single cells collected in previous studies (adult cells from ref. [23], hCS from ref. [24]) for a total of $n = 1{,}473$ cells. Cells from each of these studies were collected using identical protocols and sequencing methods. To control for unwanted variation in batch effects, all cells were normalized using Remove Unwanted Variation (RUVg) methods[58] with the following normalization genes: *CYC1, EIF4A2, SDHA, ACTB, UBC, TOP1, RPL13A, GAPDH*[59].

**Dimensionality reduction, clustering, and Monocle analysis.** All data analyses were performed using the R software (https://www.r-project.org/). Dimensionality reduction was performed in three steps. First, we calculated the overdispersion of each gene as described in ref. [60]. We then selected the top 2,000 over-dispersed genes and constructed a cell-to-cell distance matrix (1 minus absolute correlation) of all cells (using either O4 immunopanned alone, or O4 immunopanned cells along with primary human single cells from ref. [23] and ref. [24]. The distance matrix was reduced to two dimensions using *t*-SNE[25]. Clustering of groups of similar cells was performed on the two-dimensional *t*-SNE space using *k*-means. The lineage tree for the single cells was constructed using the Monocle algorithm 2.0 as described in ref. [26]. The lineage trees included all O4 immunopanned single cells as well as primary adult human OPCs and oligodendrocytes from ref. [23]. *t*-SNE plots were colored by hiPS cell line using metadata provided in the Gene Expression Omnibus accession GSE115011. These metadata were also used to determine the proportion of dividing, immature (OPCs and NFOs), and mature myelinating oligodendrocytes (as defined by the *k*-means clustering of the *t*-SNE space described above) attributed to each hiPS cell line. Correlations between hiPS cell lines were calculated using Pearson correlation values between the log normalized gene expression data for each group.

**Viral labeling and assembly of neural spheroids.** The viral infection of the 3D neural spheroids was performed as previously described[20,61]. In brief, hOLS were transferred to a 1.5-ml microcentrifuge Eppendorf tube containing 300 µl complete DMM with virus and incubated overnight. The next day, hOLS were transferred into fresh complete DMM in ultra-low attachment plates. Lentivirus (lenti-*Sox10*-MCS5::eGFP$^+$; construct reported and received from F.J. Sim[32]) was generated by transfecting HEK293T cells with Lipofectamine 2000 (Thermo Fisher, 11668019) and concentrating the supernatant with the Lenti-X concentrator (Takara Bio, 631232) 72 h later.

**Live cell imaging and analysis of *Sox10*-MCS5::eGFP $^+$ cell migration.** The migration of *Sox10*-MCS5::eGFP$^+$ cells was imaged for 8–12 h under environmentally controlled conditions (37 °C, 5% $CO_2$) in intact hOLS using a confocal microscope with a motorized stage (Leica SP8). The hOLS were transferred to a well in a 96-well glass-bottom plate (Thomas Scientific, 4580) in 200 µl complete DMM and incubated in an environmentally controlled chamber for 15–30 min before imaging. During a given recording session, up to 6 hOLS were imaged at a depth of 60–70 µm and at a rate of 13–20 min per frame.

**Real-time qPCR.** mRNA was isolated using the RNeasy Mini kit (Qiagen, 74106) and RNase-Free DNAse I kit (Thermo Fisher, 18068-015), and template cDNA was prepared by reverse transcription using the SuperScript III First-Strand Synthesis SuperMix for qRT–PCR (Thermo Fisher, 11752250). qPCR was performed using SYBR Green (Thermo Fisher, 4312704) on a ViiA7 machine (Applied Biosystems, Life Technologies). Primers used are listed in Supplementary Table 3.

**Transmission electron microscopy.** hOLS were fixed in 2% glutaraldehyde and 4% PFA in 0.1 M sodium cacodylate buffer, pH 7.4, for 1 h at room temperature. After fixation, samples were then moved to 4 °C for immediate processing. The buffer was removed and replaced with 1% $OsO_4$ in double distilled $H_2O$ ($ddH_2O$) and the hOLS were gently shaken for 1 h at 4 °C. Samples were washed 3 times for 5 min each with cold $ddH_2O$. After the third rinse the hOLS were kept in 1% uranyl acetate in $ddH_2O$, and stained for 2 h to overnight. The hOLS were then dehydrated by rinsing for 10 min each in 50% ethanol at 4 °C, 70% ethanol at 4 °C, 95% ethanol at room temperature, and 100% ethanol at room temperature. A second 10-min rinse in 100% ethanol was performed followed by a 15-min rinse in acetonitrile at room temperature. The hOLS were transferred to 1:1 acetonitrile/epon for 1 h and then to 1:2 acetonitrile/epon overnight. The following day, the hOLS were placed in 100% epon for 2–3 h and then placed in molds filled with 100% epon and allowed to settle for 4 h to overnight. The molds were then polymerized in a 65 °C oven for 24 h. Samples were sectioned and imaged using a JEOL JEM1400 120-kV transmission electron microscope.

**Electrophysiology.** Sections of hOLS at days 96–175 of differentiation were obtained using an approach we previously described[20]. Briefly, hOLS were incubated in bicarbonate-buffered artificial cerebrospinal fluid (aCSF) at 23 °C and equilibrated with a mixture of 95% $O_2$ and 5% $CO_2$. The aCSF solution contained: 126 mM NaCl, 26 mM $NaHCO_3$, 10 mM glucose, 2.5 mM KCl, 1.25 mM $NaH_2PO_4$, 1 mM $MgSO_4$, and 2 mM $CaCl_2$. Slicing was performed using a Leica VT1200 vibratome. Immediately after sectioning, slices were moved to a circulation chamber containing oxygenated aCSF at room temperature.

For patch-clamp recording, cells were identified by the presence of the *Sox10*-MCS5::eGFP fluorescent reporter using an upright microscope (Scientifica). Recording electrodes of borosilicate glass had a resistance of 4–6 MΩ when filled with internal solution. The internal solution contained: 145 mM K-gluconate, 0.1 mM $CaCl_2$, 2.5 mM $MgCl_2$, 10 mM HEPES, 0.2 mM EGTA, and 4 mM Na-phosphocreatine. Glutamatergic currents were blocked by application of NBQX (20 µM, Tocris) and APV (100 µM, Tocris), which were added to the bathing solution. Electrical simulation was delivered using a bipolar tungsten electrode (FHS) placed 100–200 µm away from a recorded cell. Stimulations were delivered to slices for 0.1 ms at 300 µV and separated by at least 10 s. Voltage-gated sodium channels were blocked by application of tetrodotoxin (TTX) (1 µM, Tocris). All recordings were performed at room temperature (25 °C). Measurements were corrected for a liquid junction potential of 12 mV.

Data were collected using a 1550A digitizer (Molecular Devices) and a 700B patch-clamp amplifier (Molecular Devices), and were acquired with pClamp 10.6 software (Molecular Devices). Data were low-pass filtered at 10 kHz and digitized at 20 kHz. Averaging, digital subtraction of null traces, and current peak detection were performed using Clampfit (Molecular Devices). Data were fitted using Origin (OriginLab).

**Lysolecithin treatment and live imaging.** Lysolecithin was dissolved at a concentration of 0.25 mg ml$^{-1}$ in complete DMM and added to day 70–75 hOLS in 1.5-ml Eppendorf tubes for 15–17 h at 37 °C. Following treatment, hOLS were rinsed twice with complete DMM. Untreated and treated hOLS were transferred to a well of a 96-well glass-bottom plate (Thomas Scientific, 4580) in 200 µl complete DMM 4–6 h after rinsing, and incubated in an environmentally controlled chamber for 15–30 min before imaging. During a given recording session, hOLS were imaged at a depth of 60–70 µm and at a rate of 10–15 min per frame for 12 h. Quantification of *Sox10*-MCS5::eGFP$^+$ disappearing cells was performed blind.

**Statistics and reproducibility.** Data are presented as mean ± s.e.m. unless otherwise indicated. Distribution of the raw data was tested for normality of distribution; statistical analyses were performed using the Student's *t*-test (two-sided), Mann–Whitney *U*-test (two-sided), or Kruskall–Wallis tests. Sample sizes were estimated empirically. One hOLS sample was removed in the qPCR analysis of *VGLUT1* in Supplementary Fig. 1j following Grubb's test for outliers ($P < 0.05$). No statistical methods were used to determine sample size, but sample sizes for each type of experiment in this study are consistent with previously published work[20,21,24,42,62,63]. For lysolecithin treatment experiments, samples were randomly distributed between the two conditions and data collection and analysis were performed blinded, and unblinded for all other experiments.

**Accession codes.** Gene expression data are available in the Gene Expression Omnibus under accession number GSE115011.

**Reporting Summary.** Further information on research design is available in the Nature Research Reporting Summary linked to this article.

## Data availability

Gene expression data have been deposited in the Gene Expression Omnibus under accession number GSE115011. The data that support the findings of this study are available on reasonable request from the corresponding author.

## References


44. Paşca, S. P. et al. Using iPSC-derived neurons to uncover cellular phenotypes associated with Timothy syndrome. *Nat. Med.* **17**, 1657–1662 (2011).
45. Yazawa, M. et al. Using induced pluripotent stem cells to investigate cardiac phenotypes in Timothy syndrome. *Nature* **471**, 230–234 (2011).
46. Gallego Romero, I. et al. A panel of induced pluripotent stem cells from chimpanzees: a resource for comparative functional genomics. *eLife* **4**, e07103 (2015).
47. Marchetto, M. C. et al. Non-cell-autonomous effect of human SOD1 G37R astrocytes on motor neurons derived from human embryonic stem cells. *Cell Stem Cell* **3**, 649–657 (2008).
48. Xue, Y. et al. Sequential regulatory loops as key gatekeepers for neuronal reprogramming in human cells. *Nat. Neurosci.* **19**, 807–815 (2016).
49. The HD iPSC Consortium. Developmental alterations in Huntington's disease neural cells and pharmacological rescue in cells and mice. *Nat. Neurosci.* **20**, 648–660 (2017).
50. Renner, M. et al. Self-organized developmental patterning and differentiation in cerebral organoids. *EMBO J.* **36**, 1316–1329 (2017).
51. Kang, S. M. et al. Efficient induction of oligodendrocytes from human embryonic stem cells. *Stem Cells* **25**, 419–424 (2007).
52. Deborde, S. et al. Schwann cells induce cancer cell dispersion and invasion. *J. Clin. Invest.* **126**, 1538–1554 (2016).
53. Xiao, D. et al. Direct reprogramming of fibroblasts into neural stem cells by single non-neural progenitor transcription factor Ptf1a. *Nat. Commun.* **9**, 2865 (2018).
54. Clarke, K. E. et al. A robust and reproducible human pluripotent stem cell derived model of neurite outgrowth in a three-dimensional culture system and its application to study neurite inhibition. *Neurochem. Int.* **106**, 74–84 (2017).
55. Greber, B. et al. FGF signalling inhibits neural induction in human embryonic stem cells. *EMBO J.* **30**, 4874–4884 (2011).
56. Amin, H. et al. Electrical responses and spontaneous activity of human iPS-derived neuronal networks characterized for 3-month culture with 4096-electrode arrays. *Front. Neurosci.* **10**, 121 (2016).
57. Picelli, S. et al. Full-length RNA-seq from single cells using Smart-seq2. *Nat. Protoc.* **9**, 171–181 (2014).
58. Risso, D., Ngai, J., Speed, T. P. & Dudoit, S. Normalization of RNA-seq data using factor analysis of control genes or samples. *Nat. Biotechnol.* **32**, 896–902 (2014).
59. Penna, I. et al. Selection of candidate housekeeping genes for normalization in human postmortem brain samples. *Int. J. Mol. Sci.* **12**, 5461–5470 (2011).
60. Fan, J. et al. Characterizing transcriptional heterogeneity through pathway and gene set overdispersion analysis. *Nat. Methods* **13**, 241–244 (2016).
61. Deverman, B. E. et al. Cre-dependent selection yields AAV variants for widespread gene transfer to the adult brain. *Nat. Biotechnol.* **34**, 204–209 (2016).
62. Thomas, C. A. et al. Modeling of TREX1-dependent autoimmune disease using human stem cells highlights L1 accumulation as a source of neuroinflammation. *Cell Stem Cell* **21**, 319–331.e8 (2017).
63. Mariani, J. et al. FOXG1-dependent dysregulation of GABA/glutamate neuron differentiation in autism spectrum disorders. *Cell* **162**, 375–390 (2015).

nature research

Corresponding author(s): Sergiu P. Pasca

# Reporting Summary

Nature Research wishes to improve the reproducibility of the work that we publish. This form provides structure for consistency and transparency in reporting. For further information on Nature Research policies, see Authors & Referees and the Editorial Policy Checklist.

## Statistical parameters

When statistical analyses are reported, confirm that the following items are present in the relevant location (e.g. figure legend, table legend, main text, or Methods section).

| n/a | Confirmed | |
|---|---|---|
| ☐ | ☒ | The exact sample size (*n*) for each experimental group/condition, given as a discrete number and unit of measurement |
| ☐ | ☒ | An indication of whether measurements were taken from distinct samples or whether the same sample was measured repeatedly |
| ☐ | ☒ | The statistical test(s) used AND whether they are one- or two-sided<br>*Only common tests should be described solely by name; describe more complex techniques in the Methods section.* |
| ☒ | ☐ | A description of all covariates tested |
| ☐ | ☒ | A description of any assumptions or corrections, such as tests of normality and adjustment for multiple comparisons |
| ☐ | ☒ | A full description of the statistics including central tendency (e.g. means) or other basic estimates (e.g. regression coefficient) AND variation (e.g. standard deviation) or associated estimates of uncertainty (e.g. confidence intervals) |
| ☐ | ☒ | For null hypothesis testing, the test statistic (e.g. *F*, *t*, *r*) with confidence intervals, effect sizes, degrees of freedom and *P* value noted<br>*Give P values as exact values whenever suitable.* |
| ☒ | ☐ | For Bayesian analysis, information on the choice of priors and Markov chain Monte Carlo settings |
| ☒ | ☐ | For hierarchical and complex designs, identification of the appropriate level for tests and full reporting of outcomes |
| ☒ | ☐ | Estimates of effect sizes (e.g. Cohen's *d*, Pearson's *r*), indicating how they were calculated |
| ☐ | ☒ | Clearly defined error bars<br>*State explicitly what error bars represent (e.g. SD, SE, CI)* |

*Our web collection on statistics for biologists may be useful.*

## Software and code

Policy information about availability of computer code

| | |
|---|---|
| Data collection | pClamp v10.6 |
| Data analysis | GraphPad Prism v7.0d, Image J v2.0.0 (FIJI), R v3.4.1, ClampFit v10.7, Origin v2018. |

For manuscripts utilizing custom algorithms or software that are central to the research but not yet described in published literature, software must be made available to editors/reviewers upon request. We strongly encourage code deposition in a community repository (e.g. GitHub). See the Nature Research guidelines for submitting code & software for further information.

## Data

Policy information about availability of data

All manuscripts must include a data availability statement. This statement should provide the following information, where applicable:

- Accession codes, unique identifiers, or web links for publicly available datasets
- A list of figures that have associated raw data
- A description of any restrictions on data availability

RNA-seq data was deposited to GEO and the accession number is GSE115011. Data are available upon request from the corresponding author.

# Field-specific reporting

Please select the best fit for your research. If you are not sure, read the appropriate sections before making your selection.

☒ Life sciences ☐ Behavioural & social sciences

For a reference copy of the document with all sections, see nature.com/authors/policies/ReportingSummary-flat.pdf

# Life sciences

## Study design

All studies must disclose on these points even when the disclosure is negative.

| | |
|---|---|
| Sample size | Sample sizes estimated empirically, based on previous studies in the field. |
| Data exclusions | One hOLS sample was removed in the qPCR analysis of VGLUT1 in Supplementary Fig. 1j following Grubb's test for outliers. This exclusion criteria was not pre-established. |
| Replication | Experiments were performed using 7 individual hiPS cell lines derived from 7 healthy subjects. For each type of experiment we collected multiple hOLS from each differentiation. Data for every type of experiment was collected from up to 4 individual differentiations of each hiPS cell line. The number of replications for each type of experiment are indicated in the manuscript in the appropriate section and in Supplementary Table 1. |
| Randomization | hOLS were randomly selected for each type of experiment. |
| Blinding | The investigators were blinded to the lysolecithin treatment of the hOLS. The investigators were not blind to the age of the hOLS. |

## Materials & experimental systems

Policy information about availability of materials

| n/a | Involved in the study |
|---|---|
| ☒ | ☐ Unique materials |
| ☐ | ☒ Antibodies |
| ☐ | ☒ Eukaryotic cell lines |
| ☒ | ☐ Research animals |
| ☐ | ☒ Human research participants |

### Antibodies

Antibodies used

anti-OLIG2 (Marchetto, Muotri et al. 2008) (rabbit, 1:500, Millipore, AB9610, Lot 2950732)

anti-NKX2-2 (Xue, Qian et al. 2016) (mouse, 1:200, DSHB, 74.5A5)

anti-PDGFRα (Consortium 2017) (rabbit, 1:500, Santa Cruz, sc-338, lot D2015)

anti-O4 (Renner, Lancaster et al. 2017) (mouse, 1:500, R&D systems, MAB1326)

anti-O1 (Kang, Cho et al. 2007) (mouse, 1:200, R&D systems, MAB1327)

anti-MBP (Deborde, Omelchenko et al. 2016) (rat, 1:300, Millipore, MAB386)

anti-GFAP (Xiao, Liu et al. 2018) (rabbit, 1:1000, Agilent DAKO, Z0334, lot 20035993)

anti-Neurofilament-H 200K (Clarke, Tams et al. 2017) (mouse, 1:500, Abcam, AB7795)

anti-GABA (Greber, Coulon et al. 2011) (rabbit, 1:1000, Sigma, A2052)

anti-MAP2 (Amin, Maccione et al. 2016) (guinea pig, 1:2500 on coverslips, 1:10000 on cryosections, Synaptic Systems, 188004)

anti-O4 hybridoma (1:2.5 dilution of 0.02% BSA produced by the Barres Lab (Zhang, Sloan et al. 2016))

---

Amin, H., A. Maccione, F. Marinaro, S. Zordan, T. Nieus and L. Berdondini (2016). "Electrical Responses and Spontaneous Activity of Human iPS-Derived Neuronal Networks Characterized for 3-month Culture with 4096-Electrode Arrays." Front Neurosci 10:

121.

Clarke, K. E., D. M. Tams, A. P. Henderson, M. F. Roger, A. Whiting and S. A. Przyborski (2017). "A robust and reproducible human pluripotent stem cell derived model of neurite outgrowth in a three-dimensional culture system and its application to study neurite inhibition." Neurochem Int 106: 74-84.

Consortium, H. D. i. (2017). "Developmental alterations in Huntington's disease neural cells and pharmacological rescue in cells and mice." Nat Neurosci 20(5): 648-660.

Deborde, S., T. Omelchenko, A. Lyubchik, Y. Zhou, S. He, W. F. McNamara, N. Chernichenko, S. Y. Lee, F. Barajas, C. H. Chen, R. L. Bakst, E. Vakiani, S. He, A. Hall and R. J. Wong (2016). "Schwann cells induce cancer cell dispersion and invasion." J Clin Invest 126(4): 1538-1554.

Greber, B., P. Coulon, M. Zhang, S. Moritz, S. Frank, A. J. Muller-Molina, M. J. Arauzo-Bravo, D. W. Han, H. C. Pape and H. R. Scholer (2011). "FGF signalling inhibits neural induction in human embryonic stem cells." EMBO J 30(24): 4874-4884.

Kang, S. M., M. S. Cho, H. Seo, C. J. Yoon, S. K. Oh, Y. M. Choi and D. W. Kim (2007). "Efficient induction of oligodendrocytes from human embryonic stem cells." Stem Cells 25(2): 419-424.

Marchetto, M. C., A. R. Muotri, Y. Mu, A. M. Smith, G. G. Cezar and F. H. Gage (2008). "Non-cell-autonomous effect of human SOD1 G37R astrocytes on motor neurons derived from human embryonic stem cells." Cell Stem Cell 3(6): 649-657.

Renner, M., M. A. Lancaster, S. Bian, H. Choi, T. Ku, A. Peer, K. Chung and J. A. Knoblich (2017). "Self-organized developmental patterning and differentiation in cerebral organoids." EMBO J 36(10): 1316-1329.

Xiao, D., X. Liu, M. Zhang, M. Zou, Q. Deng, D. Sun, X. Bian, Y. Cai, Y. Guo, S. Liu, S. Li, E. Shiang, H. Zhong, L. Cheng, H. Xu, K. Jin and M. Xiang (2018). "Direct reprogramming of fibroblasts into neural stem cells by single non-neural progenitor transcription factor Ptf1a." Nat Commun 9(1): 2865.

Xue, Y., H. Qian, J. Hu, B. Zhou, Y. Zhou, X. Hu, A. Karakhanyan, Z. Pang and X. D. Fu (2016). "Sequential regulatory loops as key gatekeepers for neuronal reprogramming in human cells." Nat Neurosci 19(6): 807-815.

Zhang, Y., S. A. Sloan, L. E. Clarke, C. Caneda, C. A. Plaza, P. D. Blumenthal, H. Vogel, G. K. Steinberg, M. S. Edwards, G. Li, J. A. Duncan, 3rd, S. H. Cheshier, L. M. Shuer, E. F. Chang, G. A. Grant, M. G. Gephart and B. A. Barres (2016). "Purification and Characterization of Progenitor and Mature Human Astrocytes Reveals Transcriptional and Functional Differences with Mouse." Neuron 89(1): 37-53.

Validation

Articles validating the used antibodies are included above.

## Eukaryotic cell lines

Policy information about cell lines

| | |
|---|---|
| Cell line source(s) | hiPS cell lines (Suppl. Table 1) were derived in the laboratory w/ IRB approval and written consent, except for one line which was obtained from the Gilad lab (details in text). |
| Authentication | hiPS cell lines were assessed for pluripotency and genomic integrity (by Cyto-SNP arrays). HEK293T was not authenticated. |
| Mycoplasma contamination | All cell lines were tested for Mycoplasma contamination and tested negative |
| Commonly misidentified lines (See ICLAC register) | No. |

## Human research participants

Policy information about studies involving human research participants

| | |
|---|---|
| Population characteristics | n/a (de-identified lines). |

# Method-specific reporting

| n/a | Involved in the study |
|---|---|
| ☒ | ☐ ChIP-seq |
| ☒ | ☐ Flow cytometry |
| ☒ | ☐ Magnetic resonance imaging |